Proceedings of 12th European Conference on Turbomachinery Fluid dynamics
Paper ID: ETC2017-133 & Thermodynamics ETC12, April 3-7, 2017; Stockholm, Sweden

USING AUTOMATED OPTIMISATION TO CALIBRATE A CORRELATION-BASED TRANSITION MODEL

C. Morsbach[1] *- M. Aulich*[2] *- F. Klingenberg*[3]

[1]Department of Numerical Methods, [2]Department of Fan and Compressor
Institute of Propulsion Technology, German Aerospace Center (DLR)
Linder Hoehe, 51147 Cologne, Germany
[1]christian.morsbach@dlr.de, [2]marcel.aulich@dlr.de
[3]Aerodynamics / Methods
MTU Aero Engines AG
Dachauer Str. 665, 80995 Munich, Germany
florian.klingenberg@mtu.de

ABSTRACT

Transition models used in turbomachinery CFD are based on empirical correlations derived from a series of fundamental test cases. When these models are applied to complex configurations they often do not perform as desired and need to be tuned to the respective area of application. In this paper, an approach to tune a correlation based transition model to a given set of turbine rigs using automated optimisation is presented. The model is optimised such that deviations from experiments in terms of blade pressure distribution and global losses are minimised. The optimisation strategy and results are analysed in detail showing strengths and weaknesses of the proposed approach. While the agreement with experimental data of the turbine rigs can be improved, an analysis of zero pressure gradient flat plate flow shows that the resulting models cannot be considered as general as the original model.

KEYWORDS

transition, automated optimisation, turbine

INTRODUCTION

The prediction of laminar to turbulent transition is essential for the appropriate description of the flow through turbine stages of turbomachines. Currently, steady Reynolds-averaged Navier-Stokes (RANS) methods are heavily employed in the industrial design process. Different approaches exist to model transition. One approach is phenomenological modeling based on the concept of laminar kinetic energy (Walters & Cokljat, 2008). Another school employs correlations based on experimental data which are calibrated using basic test cases such as the flow over flat plates. In principle, these correlations can be exchanged for ones which more accurately describe the range of flows in the desired area of application of the model. The γ-Re_θ model (Menter *et al.*, 2006) is a representative model for this class.

The correlations are functional dependencies with parameters, whose manual calibration represents a large effort (e.g. Insinna *et al.*, 2014). It requires a thorough understanding of the transition model and the physical flow phenomena to perform the task in a reasonable time frame considering the large parameter space. Our proposition is to use an automated optimisation tool to find the optimal set of parameters for a given form of correlation and set of flow test cases.

Only very recently has a similar approach been published by Minot *et al.* (2016). They optimised the transition model using the T106C turbine cascade at three different turbulence intensities and five respective operating points. A linear combination of error in isentropic Mach number and Reynolds lapse rate served as a single objective function. In contrast to our approach, they optimised the correlations for $Re_{\theta c}$ and F_{length}, only. They demonstrated that their improved model did not deteriorate the prediction of heat transfer in the VKI LS 89 high pressure turbine case.

We implemented a process based on DLR's optimiser AutoOpti, which has been developed for multi-objective optimisations using an evolutionary strategy accelerated by surrogate models (Siller *et al.*, 2009; Aulich & Ulrich, 2011). The CFD simulations are performed using DLR's flow solver for turbomachinery applications TRACE (Becker *et al.*, 2010). TRACE is a density-based finite volume solver. The Reynolds stress tensor is modelled by the Menter SST k-ω turbulence model (Menter *et al.*, 2003) coupled with the γ-Re_θ transition model. The coefficients used by the latter can be controlled by the optimiser.

The set of test cases consists of several relevant turbomachinery rigs, for which high quality experimental data are available. The agreement of the simulation results with the experimental data is translated to objective functions and restrictions for the optimiser. These have been formulated involving data such as the blade pressure distribution, the Reynolds lapse rate as well as relations between lapse rates of different rigs. We investigate different optimisation strategies combining different objective functions and show that the agreement of the computed results with the measurement data can be improved.

METHOD

Physical modelling

This section introduces the employed RANS turbulence and transition models to highlight which parts of the model are modified in the optimisation. Turbulence is modelled using the Menter SST k-ω model (Menter *et al.*, 2003). To remedy problems with excessive production of turbulent kinetic energy at stagnation points, its production term is formulated according to Kato & Launder (1993). Laminar to turbulent transition is modelled using the γ-Re_θ (Menter *et al.*, 2006). The model determines the intermittency, which is used to control the source terms of the turbulence model, by the transport equation

$$\frac{D\rho\gamma}{Dt} = \frac{\partial}{\partial x_j}\left[\left(\mu + \sigma_\gamma \mu_T\right)\frac{\partial \gamma}{\partial x_j}\right] + F_{\text{length}} c_{a1} \rho S (\gamma F_{\text{onset}})^{c_\alpha}(1 - c_{e1}\gamma) + c_{a2}\rho W \gamma F_{\text{turb}}(1 - c_{e2}\gamma) \tag{1}$$

with the strain norm S and vorticity norm W. We follow the nomenclature of model coefficients used by Malan *et al.* (2009) with some minor modifications for consistency. The source terms are given by

$$F_{\text{onset}} = \max\left\{\min\left[\max\left(F_{\text{onset1}}, F_{\text{onset1}}^4\right), 2\right] - F_{\text{onset3}}, 0\right\}, \quad F_{\text{turb}} = \exp\left[-\left(\frac{Re_T}{4}\right)^4\right] \tag{2}$$

with

$$F_{\text{onset1}} = \frac{Re_\nu}{2.193 Re_{\theta c}}, \quad F_{\text{onset3}} = \max\left[1 - \left(\frac{Re_T}{2.5}\right)^3, 0\right], \quad Re_\nu = \frac{\rho S y^2}{\mu}, \quad Re_T = \frac{\rho k}{\mu \omega}. \tag{3}$$

Table 1: **Free parameters of the γ-Re_θ model.**

Parameter	lower bound	initial value	upper bound	Parameter	lower bound	initial value	upper bound
c_α	0.33	0.5	0.99	σ_γ	0.5	1.0	10.0
c_{a1}	1.0	2.0	15.0	σ_{Re_θ}	0.5	10.0	20.0
c_{e1}	0.5	1.0	1.5	C_1	0.1	0.615	1.0
c_{a2}	0.01	0.03	0.08	C_2	25.0	61.5	100.0
c_{e2}	10.0	50.0	100.0	$F_{\text{length},1}$	5.0	7.168	15.0
$c_{\theta t}$	0.001	0.03	0.05	$F_{\text{length},2}$	0.01	0.01173	0.05
c_{t}	0.5	500.0	1000	$F_{\text{length},3}$	0.1	0.5	1.0
s_1	1.0	8.0	10.0	$F_{\text{length},4}$	200.0	300.0	500.0
s_2	1.0	2.0	5.0				

A further transport equation

$$\frac{D\rho\tilde{Re}_{\theta t}}{Dt} = \frac{\partial}{\partial x_j}\left[\sigma_{Re_\theta}\left(\mu+\mu_T\right)\frac{\partial\tilde{Re}_{\theta t}}{\partial x_j}\right] + c_{\theta t}\frac{(\rho U)^2}{c_t\mu}(Re_{\theta t}-\tilde{Re}_{\theta t})(1-F_{\theta t}) \tag{4}$$

with $U=\sqrt{U_iU_i}$ and

$$F_{\theta t} = \min\left\{\max\left[F_{\text{wake}}\exp\left[-\left(\frac{U^2}{375W\nu\tilde{Re}_{\theta t}}\right)^4\right], 1-\left(\frac{c_{e2}\gamma-1}{c_{e2}-1}\right)^2\right], 1\right\} \tag{5}$$

with

$$F_{\text{wake}} = \exp\left[-\left(\frac{Re_\omega}{10^5}\right)^2\right], \quad Re_\omega = \frac{\rho\omega y^2}{\mu} \tag{6}$$

is used to supply the non-local Reynolds number based on momentum thickness locally to empirical correlations.

The model uses three empirical correlations to determine the onset (F_{onset}) and range (F_{length}) of transition. Only the correlation for the transition onset momentum thickness Reynolds number $Re_{\theta t}$ was published in the original paper. In a later paper, Langtry & Menter (2009) published the remaining correlations for critical Reynolds number $Re_{\theta c}$ and the function F_{length}. We use the correlations by Malan *et al.* (2009)

$$Re_{\theta c}(\tilde{Re}_{\theta t}) = \max\left[\min\left(C_1\tilde{Re}_{\theta t}+C_2, \tilde{Re}_{\theta t}\right), 20\right] \tag{7}$$

$$F_{\text{length}}(\tilde{Re}_{\theta t}) = \min\left[\exp\left(F_{\text{length},1}-F_{\text{length},2}\tilde{Re}_{\theta t}\right)+F_{\text{length},3}, F_{\text{length},4}\right], \tag{8}$$

which are formulated with less degrees of freedom C_i and $F_{\text{length},i}$ for the present optimisation. Finally, the effective intermittency used in the turbulence model is computed by $\gamma_{\text{eff}} = \max(\gamma, \gamma_{\text{sep}})$ with

$$\gamma_{\text{sep}} = \min\left[s_1\max\left(\frac{Re_v}{3.235Re_{\theta c}}-1, 0\right)F_{\text{reattach}}, s_2\right]F_{\theta t}, \quad F_{\text{reattach}} = \exp\left(-\left(\frac{Re_T}{20}\right)^4\right) \tag{9}$$

accounting for separation induced transition. Tab. 1 summarises the allowed ranges of the free optimisation parameters and their respective initial values.

Test cases

The experimental data used for the calibration are a keystone of the process because they should cover the desired application area of the transition model as broadly as possible. Five different low pressure turbine (LPT) blade geometries were selected, which cover together the design range in question. The first two geometries are MTU-T160, a design typical for the legacy LPT generation (Gier & Hübner, 2005) and a high lift variant of this blade with a large separation bubble on the suction side. The remaining three cascades are up-to-date designs: a high lift design with conventional load, a reduced diffusion and a forward load design. The latter are used in recent engine designs and therefore not published in more detail.

The measurement data were obtained by high-speed cascade wind tunnel tests operated at several different Reynolds numbers respectively. The obtained table-structured, high-quality data represent the full range of typical geometries and operating conditions with regard to the transition behaviour in actual LPTs.

Only a mid-section of the turbine rigs is simulated in the optimisation process to save computation time. While the blade walls are meshed with low Reynolds resolution, the hub and tip walls are treated as inviscid walls and shaped to obtain the correct AVDR of the experiments. Constant values of stagnation pressure and temperature, inflow angle, turbulence intensity and length scale are prescribed at the inlet and a constant pressure is set at the outlet. Each operating point is automatically post-processed to obtain the isentropic Mach number $M_{\text{is}}(p_{t1}, p(x/c_a))$ at mid-span and the total pressure loss coefficient $\zeta = (p_{t1} - p_{t2})/(p_{t2} - p_2)$ based on the inlet stagnation pressure p_{t1}, the outlet stagnation and static pressure p_{t2} and p_2 and the static pressure on the blade surface p.

Objective functions

In the following, the objective functions are described. They condense the deviation of the computational results from the experimental data of the set of N_{cases} turbine rigs into single numbers. The Reynolds lapse rate of rig i, given by the total pressure loss $\zeta(Re)$ as a function of the outlet Reynolds number, is used in both optimisations. It consists of $N_{Re,i}$ operating points with a respective total pressure loss ζ_{ij}. Due to a varying number of operating points per rig, the objective function

$$\Delta\zeta = \sum_{i=1}^{N_{\text{cases}}} \frac{1}{N_{Re,i}} \sum_{j=1}^{N_{Re,i}} \left(\zeta_{ij}^{\text{sim}} - \zeta_{ij}^{\text{exp}}\right)^2 \tag{10}$$

is defined using the average squared distance from the experimental values. The second objective function is based on the pressure distribution on the blade expressed as isentropic Mach number $M_{\text{is}}(x/c_a)$. In contrast to the lapse rate, experimental and computational data points do not coincide at the same axial position x/c_a. Hence, the distance is measured between the experimental data point and the interpolated computational value at the axial position of the former as illustrated in Fig. 1 (*left*). Since the number of data points is the same for each operating point of the same rig, no averaging is required and the total objective function is given by

$$\Delta M_{\text{is}} = \sum_{i=1}^{N_{\text{cases}}} \frac{1}{N_{Re,i}} \sum_{j=1}^{N_{Re,i}} \sum_{k=1}^{N_{M_{\text{is}},ij}} \left[M_{\text{is},ijk}^{\text{sim}}\left(x_{ijk}^{\text{exp}}/c_{a,i}\right) - M_{\text{is},ijk}^{\text{exp}}\left(x_{ijk}^{\text{exp}}/c_{a,i}\right)\right]^2. \tag{11}$$

While the above functions connect computed data with measured data for each turbine rig, the following function represents computed relations between the lapse rates of different rigs.

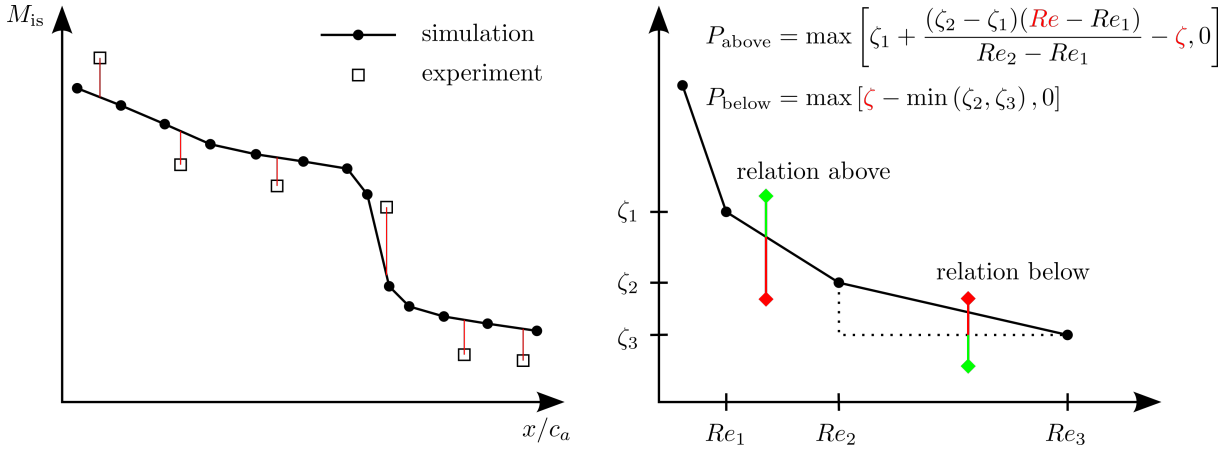

Figure 1: **Evaluation of objective function based on the isentropic Mach number M_{is} (*left*) and the relation between two Reynolds lapse rate curves $\zeta(Re)$ (*right*).**

The general idea is that the transition model should be able to rank different classes of airofoils in the correct order. For this purpose, the measured lapse rates were analysed and relations between them derived. Each point j on each measured lapse curve is compared to the other lapse curves to store its relation to the respective curve which can be either *above* or *below*. The lapse curves predicted by the CFD should reflect the relations found in the measurements. A penalty function

$$P = \sum_{j}^{N_{\text{above}}} P_{\text{above},j} + \sum_{j}^{N_{\text{below}}} P_{\text{below},j} \tag{12}$$

is designed to yield positive values if the computed lapse rates violate the measured relations. Because the loss curves are convex, the cases are treated differently to obtain a conservative expression. Fig. 1 (*right*) shows the two cases with the reference lapse curve obtained by CFD drawn in black. A point (Re_j, ζ_j) which is supposed to be above the reference curve is compared to the interpolated value between the neighbouring points (Re_i, ζ_i) and (Re_{i+1}, ζ_{i+1}). If the point is incorrectly located below the reference curve (red diamond), this results in a positive contribution to the penalty function

$$P_{\text{above},j} = \max\left[\zeta_i + \frac{(\zeta_{i+1} - \zeta_i)(Re_j - Re_i)}{Re_{i+1} - Re_i} - \zeta_j, 0\right], \tag{13}$$

which is the difference to the interpolated value on the reference curve, and no contribution if the relation is correctly predicted by the model (green diamond). A point which is supposed to be below the reference curve is compared to the minimum value of the neighbouring points yielding the penalty function

$$P_{\text{below},j} = \max\left[\zeta_j - \min\left(\zeta_i, \zeta_{i+1}\right), 0\right] \tag{14}$$

with a positive contribution according to the distance from the minimum value if the point is incorrectly located above (red diamond) and no contribution if the relation is predicted correctly (green diamond).

Optimisation strategy

Two different strategies of combining the above objective functions were employed. Both cases were multi-objective optimisations where both objective functions are driven towards a global minimum by the optimiser. The first case was based on the error in lapse rate $\Delta\zeta$ (10) and the error isentropic Mach number ΔM_{is} (11). The second case focussed on the lapse rate $\Delta\zeta$ (10) and the relations between the lapse rates represented by P (12).

After a random initialisation, all parameter sets are created in a surrogate model assisted sub-optimisation (Kriging and Bayesian neural networks). Inside this sub-optimisation parameter sets are generated by a parallelised evolutionary algorithm. The time consuming CFD calculations are replaced by the fast response of the surrogate models allowing to evaluate many parameter sets. At the end of the sub-optimisation the best parameter set is sent to a slave process where the CFD simulations are performed. Expected values and uncertainties of both objective functions are combined in the Expected Volume Gain criterion (Aulich *et al.*, 2014; Voß *et al.*, 2014). In a two dimensional objective space, the Expected Volume Gain is the expected area between the Pareto front and the predicted objectives of a newly created parameter set. Inside the sub-optimisation the Expected Volume Gain is maximised.

200 samples are created randomly in the parameter space before starting the surrogate assisted process. Every ten CFD assessed parameter sets the surrogate models are updated in a training process. The training process is not performed in every sub-optimisation to reduce CPU time. In the first optimisation, the two objective functions $\Delta\zeta$ and ΔM_{is} are approximated directly by surrogate models. In the second optimisation each point of a lapse rate curve is predicted by a surrogate model. This results in 27 different surrogate models. The objective function $\Delta\zeta$ and the penalty function P, which is used as second objective function, are calculated from the surrogate model predictions. While this surrogate approach is more time consuming, it increases the quality of the approximation.

RESULTS AND DISCUSSION

As both optimisations had two respective objective functions, no single best result can be stated. Instead, Fig. 2 shows the Pareto fronts, normalised with respect to the initial parameter set, for optimisation 1 using the lapse rate $\Delta\zeta$ and pressure distribution ΔM_{is} (*left*) and optimisation 2 using the lapse rate $\Delta\zeta$ and relations between lapse rates P (*right*). Each point (member) represents a set of model coefficients and is coloured by its Pareto rank. Rank 1 members are defined such that they are better in all objective functions than members with a greater rank and that no rank 1 member is better than any other rank 1 member in all objective functions. We will use the Pareto front to choose members which are very good in one of the respective objectives and ones which represent a compromise. These members will be checked for the prediction accuracy of the T160 turbine rig as well as the zero pressure gradient flat plate T3 series (Roach & Brierley, 1992). They are marked in the respective plots with their number which represents the instance at which they were created.

Optimisation 1 was stopped after the assessment of 2521 members. Member 733, which represents the best result with respect to the deviation in pressure distributions, was created relatively early. Later in the optimisation, the focus of creation was in the region representing a compromise between deviation in pressure distribution and lapse rate. We will compare results of the T160 rig for members 733 (very good with respect to ΔM_{is}), 1964 (very good with respect to $\Delta\zeta$) and 2313 (good compromise) with the initial member 0 and experimental data. When interpreting the results of a single turbine rig, it has to be considered that the position on

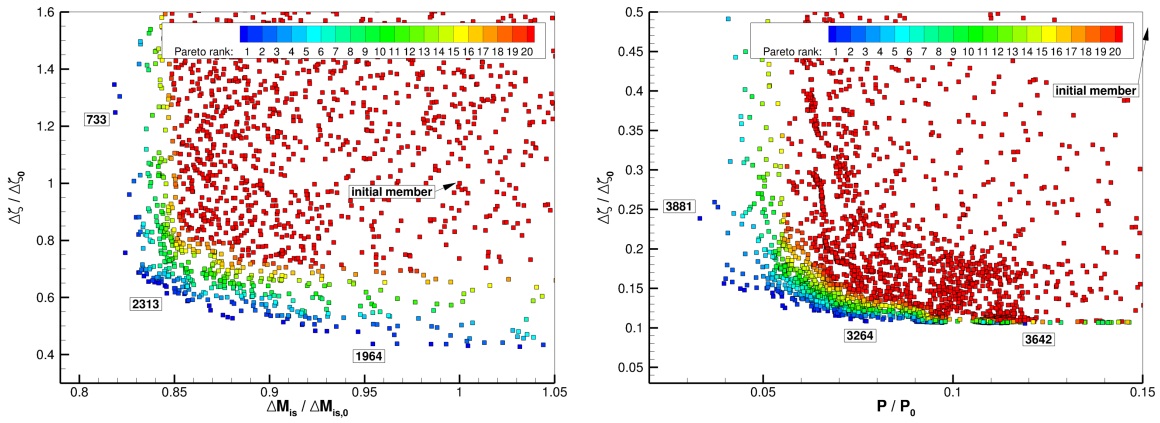

Figure 2: **Optimisation results in terms of normalised objective functions for optimisation 1 based on $\Delta\zeta$ and ΔM_{is} (*left*) and optimisation 2 based on $\Delta\zeta$ and P (*right*).**

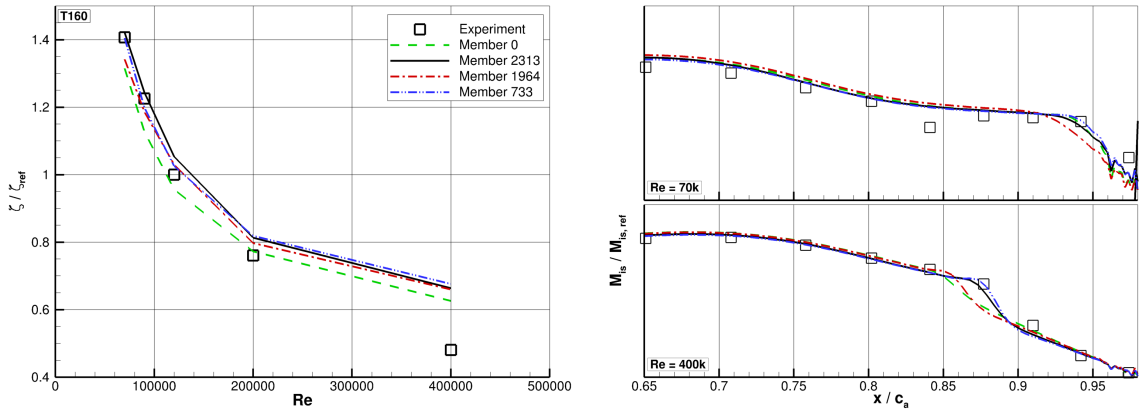

Figure 3: **T160 lapse rate (*left*) and suction side pressure distribution (*right*) of selected Pareto rank 1 members of optimisation 1 compared to the initial model and experiments.**

the Pareto front represents the deviation over all turbine rigs.

Fig. 3 (*left*) shows the lapse rate with the loss coefficient normalised with the reference loss value at $Re = 120k$. The initial model underestimates the losses for smaller Reynolds numbers. All optimised models can clearly improve the prediction in this region. On the other hand, at higher Reynolds numbers, the deviation from the experiment is increased compared to the initial model with the least increase, as expected, for member 1964. The pressure distribution on the aft part of the blade suction side is shown in Fig. 3 for the lowest Reynolds number (*top right*) and the highest Reynolds number (*bottom right*) of this case. At $Re = 400k$ it can be clearly seen that the members with a small deviation ΔM_{is} show an improved prediction of the separation bubble.

For optimisation 2, which was stopped after 3990 members, the equivalent results are not plotted due to space constraints. Since the pressure distribution was no objective function, no significant differences could be observed between the selected Pareto rank 1 members. They

all improved the prediction of the pressure distribution for $Re = 400k$ compared to the initial member. The agreement with the measured data of the lapse rate reflected the member's respective position on the Pareto front. Concerning the relations between lapse rates of different turbine rigs, great improvements could be obtained compared to the initial member, which failed 24 of 61 relations. The Pareto rank 1 members failed to meet only 4-8 of the 61. The three selected members cover this range with the best compromise meeting 56 relation criteria.

Fig. 4 investigates the variation in the model correlations and coefficients for the Pareto rank 1 members of both optimisations. On the left hand side, the correlations $Re_{\theta C}$ and F_{length} are shown. For optimisation 1 (blue), the critical Reynolds number $Re_{\theta C}$ is equal to $Re_{\theta t}$ for all members in contrast to the original model (green) which reduces the slope at $Re = 160$. In optimisation 2 (red), the best members reduce the slope between $Re = 370$ and 470 to a similar value. On the other hand, significant scatter can be observed in the correlations for F_{length} with a clustering around one shape of exponential functions with different cut-off values. All optimised correlations disagree with the initial correlation with one exception. The point at which the constant value changes to an exponential decay is around the initial value of $Re = 125$.

Fig. 4 (*right*) shows an analysis of the optimised values for the remaining free model coefficients. The plot shows the scaled value of each coefficient with respect to the intervals specified in Tab. 1 for the complete set of Pareto rank 1 members of each optimisation. Each member is visualised with a grey vertical marker and the shaded areas are probability density functions derived from the complete set of values. For reference, the coefficients of the initial member and one member representing the best compromise between the two objective functions for each optimisation are plotted. Different observations can be made in this plot. Firstly, there are parameters for which the optimiser can find a value within a narrow band in contrast to others which vary over almost the complete allowed range and seem to be much less sensitive in view of the set of test cases and objective functions. The former are especially the coefficients s_1 and s_2, responsible for separation induced transition, $c_{\theta t}/c_t$, controlling the magnitude of the source term in the $\tilde{Re}_{\theta t}$ equation, and c_{e1} one of the destruction coefficients of the γ equation. Other parameters such as the diffusion coefficient of the γ equation σ_γ or the exponent c_α of the γ source term vary broadly. Secondly, some parameters have a very different influence depending on the choice of objective function. The separation parameter s_1 and the diffusion coefficient σ_{Re_θ}, for example, are optimised to a very narrow interval for optimisation 2 while their values cover significantly larger ranges for optimisation 1. This could be due to the large number of cases with separation bubbles for which s_1 and s_2 have a major influence on the pressure distribution. Thirdly, one class of parameters shows overlapping intervals for both choices of objective functions while others are disjunctive. Finally, as shown for the correlation functions, the set of best parameters for either choice of objective functions differs significantly from the initial model. This indicates that not only need the correlations but also the model coefficients be adapted when the model is tuned.

The question which remains to be answered is if the model coefficients especially tuned for the five turbine rigs can still be used in a more general context. For this reason, we computed three cases of the ERCOFTAC T3 series flat plate with zero pressure gradient (Roach & Brierley, 1992). The results are shown in Fig. 5 for optimisation 1 (*left*) and 2 (*right*). The initial model predicts the correct transition location for the cases T3A and T3B and a slightly premature transition for T3A-. All selected members from optimisation 1 shift the transition location upstream for the first two cases and no transition can be found for T3A- within the length of the computed geometry. Optimisation 2 shows a similar result for the T3B and T3A-

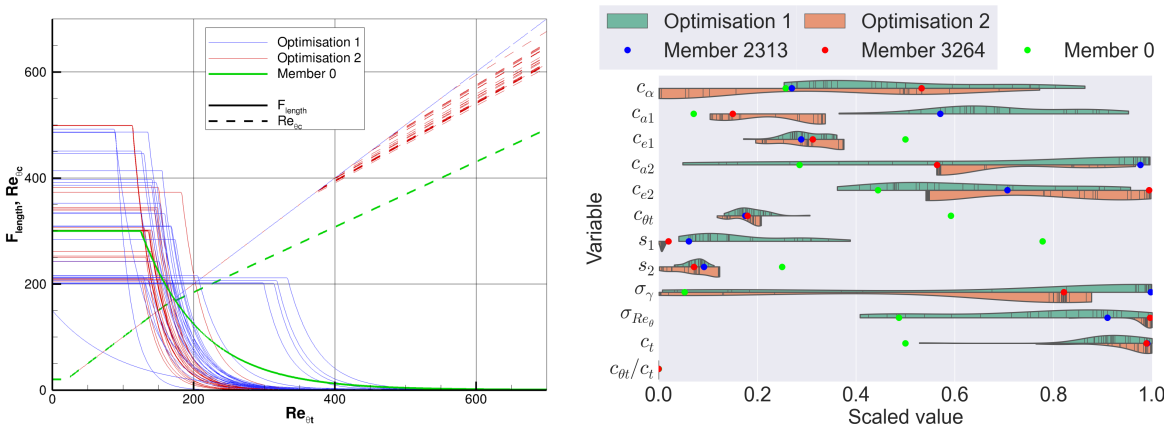

Figure 4: **Variation of the correlations $F_{\mathbf{length}}$ and $Re_{\theta c}$ (*left*) and transport equation coefficients (*right*) for Pareto rank 1 members compared to the initial model.**

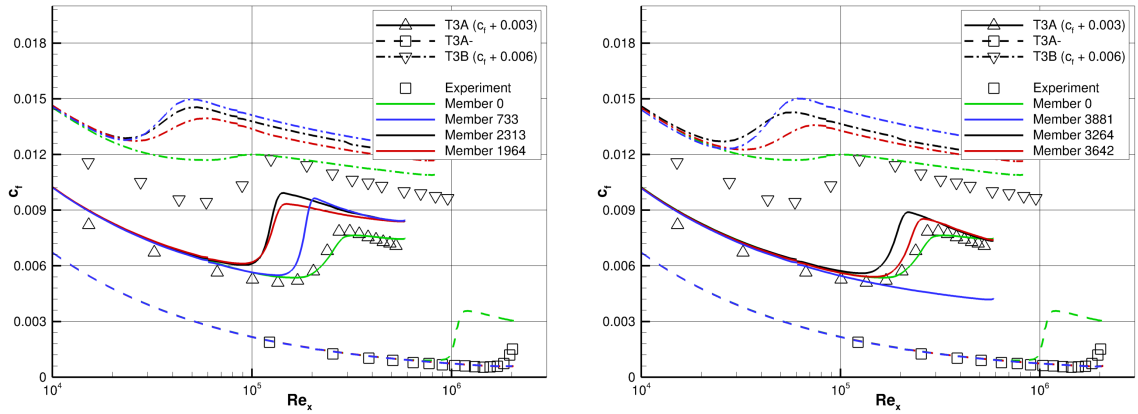

Figure 5: **Skin friction coefficient c_f of ZPG flat plate flow (Roach & Brierley, 1992) for selected Pareto rank 1 members of optimisation 1 (*left*) and optimisation 2 (*right*).**

cases. Members 3264 and 3642 with a very good agreement concerning the lapse rate $\Delta\zeta$ show less deviation from the experiments and the initial model for T3A. Only member 3881 with a comparably large deviation in $\Delta\zeta$ shows a completely laminar skin friction distribution. It can be said that the model optimised for the selected turbine rigs loses generality and shows a deteriorated prediction of the basic flat plate test case.

CONCLUSIONS

The correlations and coefficients of the γ-Re_θ transition model coupled to the Menter SST k-ω turbulence model have been automatically optimised for five turbine rigs on the basis of different objective functions. A definite improvement of the prediction quality over the set of test cases can be achieved compared to the initial set of parameters. This improvement, however, comes at the expense of a deteriorated prediction of the transition in ZPG flat plate flow. While the model can be successfully tuned to a very specific set of test cases, this study suggests that

more topologically different test cases should be included in the optimisation in order to obtain a more general model. Future work will include more basic test cases and investigate objective functions directly related to the positions of separation bubbles on the blades.

ACKNOWLEDGEMENTS

This work was financed by the German *Bundesministerium für Wirtschaft und Technologie* under the grant number 20T1302B.

REFERENCES

Aulich, Marcel & Ulrich, Siller 2011 High-dimensional constrained multiobjective optimization of a fan stage. In *ASME Turbo Expo 2011*.

Aulich, Marcel, Voß, Christian & Raitor, Till 2014 Optimization strategies demonstrated on a transonic centrifugal compressor. In *ISROMAC 15*.

Becker, Kai, Heitkamp, Kathrin & Kügeler, Edmund 2010 Recent progress in a hybrid-grid CFD solver for turbomachinery flows. In *V European Conference on Computational Fluid Dynamics ECCOMAS CFD 2010*. Lisbon, Portugal.

Gier, Jochen & Hübner, Norbert 2005 Design and analysis of a high stage loading five-stage lp turbine rig employing improved transition modeling. In *ASME Turbo Expo 2005: Power for Land, Sea, and Air*, , vol. 6, pp. 759–769.

Insinna, Massimiliano, Griffini, Duccio, Salvadori, Simone & Martelli, Francesco 2014 Film cooling performance in a transonic high-pressure vane: Decoupled simulation and conjugate heat transfer analysis. *Energy Procedia* **45**, 1126 – 1135.

Kato, M. & Launder, B. E. 1993 The modeling of turbulent flow around stationary and vibrating square cylinders. In *9th Symposium on Turbulent Shear Flows*, pp. 10.4.1–10.4.6.

Langtry, Robin & Menter, Florian 2009 Correlation-based transition modeling for unstructured parallelized computational fluid dynamics codes. *AIAA J.* **47** (12), 2894–2906.

Malan, Paul, Suluksna, Keerati & Juntasaro, Ekachai 2009 Calibrating the γ-Re_θ transition model for commercial CFD. In *Aerospace Sciences Meetings*. American Institute of Aeronautics and Astronautics.

Menter, F., Kuntz, M. & Langtry, R. 2003 Ten years of industrial experience with the SST model. In *Turbulence, Heat and Mass Transfer 4* (ed. K. Hanjalić, Y. Nagano & M. Tummers).

Menter, F. R., Langtry, R. B., Likki, S. R., Suzen, Y. B., Huang, P. G. & Volker, S. 2006 A correlation-based transition model using local variables—part I: Model formulation. *J. Turbomach.* **128** (3), 413–422.

Minot, A., Sala El-Din, I., Barrier, R., Boniface, J.-C. & Marty, J 2016 Improvement of laminar-turbulent transition modeling within a low-pressure turbine. In *Proceedings of the ASME Turbo Expo 2016*.

Roach, P.E. & Brierley, D.H. 1992 The influence of a turbulent free stream on zero pressure gradient transitional boundary layer development. part 1: testcases T3A and T3B. In *Numerical Simulation of Unsteady Flows and Transition to Turbulence* (ed. O. Pironneau, W. Rode & I.L. Ryhming). Cambridge University Press.

Siller, Ulrich, Voß, Christian & Nicke, Eberhard 2009 Automated multidisciplinary optimization of a transonic axial compressor. In *47th AIAA Aerospace Sciences Meeting*.

Voß, Christian, Aulich, Marcel & Raitor, Till 2014 Metamodel assisted aeromechanical optimization of a transonic centrifugal compressor. In *ISROMAC 15*.

Walters, D. K. & Cokljat, D. 2008 A three-equation eddy-viscosity model for reynolds-averaged navier-stokes simulations of transitional flow. *Journal of Fluid Enginnering* **130**, 121401.1–121401.14.